SMC-TR-99-26

AEROSPACE REPORT NO.
TR-99(1222)-1

Graphite Epoxy Motor Case Impact Monitoring and Reference Strain Measurement Using Conventional Resistance Strain Gages

30 August 1999

Prepared by

L. H. WIEDEMAN
Mechanics and Materials Technology Center
Technology Operations

Prepared for

SPACE AND MISSILE SYSTEMS CENTER
AIR FORCE MATERIEL COMMAND
2430 E. El Segundo Boulevard
Los Angeles Air Force Base, CA 90245

Engineering and Technology Group

THE AEROSPACE CORPORATION
El Segundo, California

This report was submitted by The Aerospace Corporation, El Segundo, CA 90245-4691, under Contract No. F04701-93-C-0094 with the Space and Missile Systems Center, 2430 E. El Segundo Blvd., Los Angeles Air Force Base, CA 90245. It was reviewed and approved for The Aerospace Corporation by P. D. Fleischauer, Principal Director, Mechanics and Materials Technology Center. Capt. Cary Gunn was the project officer.

This report has been reviewed by the Public Affairs Office (PAS) and is releasable to the National Technical Information Service (NTIS). At NTIS, it will be available to the general public, including foreign nationals.

This technical report has been reviewed and is approved for publication. Publication of this report does not constitute Air Force approval of the report's findings or conclusions. It is published only for the exchange and stimulation of ideas.

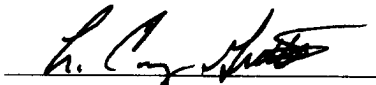

Capt. Cary Gunn
SMC/CLM

REPORT DOCUMENTATION PAGE

Form Approved
OMB No. 0704-0188

1. AGENCY USE ONLY (*Leave blank*)	2. REPORT DATE	3. REPORT TYPE AND DATES COVERED
	30 August 1999	

4. TITLE AND SUBTITLE
Graphite Epoxy Motor Case Impact Monitoring and Reference Strain Measurement Using Conventional Resistance Strain Gages

5. FUNDING NUMBERS
F04701-93-C-0094

6. AUTHOR(S)
L. H. Wiedeman

7. PERFORMING ORGANIZATION NAME(S) AND ADDRESS(ES)
The Aerospace Corporation
Technology Operations
El Segundo, CA 90245-4691

8. PERFORMING ORGANIZATION REPORT NUMBER
TR-99(1222)-1

9. SPONSORING/MONITORING AGENCY NAME(S) AND ADDRESS(ES)
Space and Missile Systems Center
Air Force Materiel Command
2430 E. El Segundo Boulevard
Los Angeles Air Force Base, CA 90245

10. SPONSORING/MONITORING AGENCY REPORT NUMBER
SMC-TR-99-26

11. SUPPLEMENTARY NOTES

12a. DISTRIBUTION/AVAILABILITY STATEMENT
Approved for public release; distribution unlimited

12b. DISTRIBUTION CODE

13. ABSTRACT (*Maximum 200 words*)

A series of low-energy impacts (below damage threshold) was monitored on subject graphite epoxy motor cases using conventional strain gages. Similar impact tests were done on an empty case and a Delta GEM inert-propellant-loaded case. The conventional strain gages were also used to monitor case bending during lifting, handling, and transportation shock exercises. The impact test energies ranged between 1 and 6 ft-lb with a 5/8-in. tup. The 6 ft-lb impacts impart a sufficiently large strain wave to be sensed by all gages on the inert loaded motor, regardless of location or orientation. This includes impacts on the cork covering. However, the strain signals for some of the remote impacts are pushing the lower limit of detection for this system (1 micro-strain). Typical strains measured for a 6 ft-lb impact on the inert-loaded case were 15 micro-strain where the gage was located 17 in. from the impact. The strain impulse damping with distance is roughly exponential for the sharp impulse and very slight for the lower-frequency ringing.

The strain waves have remarkably reproducible amplitudes and shapes for successive impacts at a given location and energy. However, the recorded waves are dependent on factors such as the orientation of the gage with respect to the case (axial vs. circumferential), the mode and direction of the wave propagation, and the location of the impact. These factors make it difficult to predict the exact wave shape for an arbitrary combination of impact location and gage orientation. The lifting exercises produced strain signals of 200 to 500 micro-strain, which are much larger than the impact strain signals. The strapping of the motor to the truck bed also imposed a significant strain offset (80 micro-strain) to the dynamic signal monitoring. Running the truck over a series of wooden 2 x 4's produced dynamic strain oscillations of ±100 micro-strain with a nominal bandwidth of 10 Hz. This large dynamic background signal would make it difficult to separate an impact strain signal from a "transportation and handling" signal.

14. SUBJECT TERMS	15. NUMBER OF PAGES
Delta Graphite Epoxy Motor, Impact sensing, Strain measurement	13
	16. PRICE CODE

17. SECURITY CLASSIFICATION OF REPORT	18. SECURITY CLASSIFICATION OF THIS PAGE	19. SECURITY CLASSIFICATION OF ABSTRACT	20. LIMITATION OF ABSTRACT
UNCLASSIFIED	UNCLASSIFIED	UNCLASSIFIED	

Acknowledgments

This report documents only one portion of a larger project to characterize different diagnostic techniques for detection of impacts on Gr/Ep motor casings. I would like to acknowledge all of the other Aerospace participants including: Ernie Robinson, Richard Welle, Dick Chang, Tom Albright, Jon Osborn, Lt. Brett Brown, Sherwin Amimoto, Eric Fournier, Charles Klimcak, Jim Nokes, and Paul Joseph.

Special thanks to the Delta Program Office and the people from AFRL/PRRO for support at Edwards AFB.

Contents

Figures

Table

1. Introduction

The failure of a strap-on graphite-epoxy solid rocket motor (GEM) caused the loss of a Delta II rocket in 1997. This failure might be attributable to impact damage suffered during handling or shipping and not detected by the pre-flight inspection. This possible cause for vehicle loss has spurred an interest in both impact damage thresholds and technologies that can provide continuous heath monitoring for flight hardware. In a project funded by the Delta Program Office, a series of tests was conducted by several personnel at The Aerospace Corporation to evaluate the utility of various monitoring systems for detecting potentially damaging impacts on graphite/epoxy (Gr/Ep) cases during handling. Sensor systems that have been proposed for the monitoring application include fiber-optic Bragg strain gages, conventional bonded-foil strain gages, accelerometers, and acoustic emission detectors. This report documents the reference resistance strain gage data taken during a series of low-energy impacts (below damage threshold) on two subject Gr/Ep cases. Data from the Delta Program Office indicated that the damage threshold for a loaded GEM was 7 to 9 ft-lb with a 5/8-in. tup. For this reason, impacts on both cases were limited to a maximum energy of 6 ft-lb. The first Gr/Ep case was an empty shell located at Aerospace and was used primarily to refine the impact detection techniques. The second case was an inert-propellant-loaded Delta GEM located at Edwards AFB.

2. Experimental

The reference strain measurements were made with standard laboratory equipment. The ensemble includes Micro-Measurements rosette gages (P/N CEA-00-250UR-350) bonded to the case with M-Bond AE-10, and Micro-Measurement 3110 strain gage signal conditioner amplifier. The signal conditioner was typically set to 10 V excitation drive, 10,000 gain, and 10 kHz band-pass filter, and wired as a 1/4 bridge circuit using the internal 350-ohm resistors. For this experiment, unshielded cable was used successfully. However, this is not recommended since it is vulnerable to picking up RF noise from a host of uncharacterized sources. Three independent, 3110 signal conditioners were used in parallel to simultaneously drive the three gages on the rosette. The output signals were recorded at 8,000 points/s along with the output from a load cell located between the impact tup and the dead-weight. A circular data acquisition buffer was used to allow pre-trigger data to be included with each impact waveform. The data were digitized with a National Instruments MXIO-16F card and driven with "C" code running on a 486, 33 MHz desktop computer. The impact locations were chosen in an attempt to de-couple axial vs. circumferential wave propagation. A listing of the impacts can be found in Table 1, and a visual reference is provided by the experimental map. Points #3 and #12 were chosen as "maximum distance from the gage" impact points. All plots include a short section (negative time) of "pre-impact" points to show the baseline signal to noise limit.

Table 1. Impact Location and File Number Reference

Test No.	Location Map	Strain Gage and File No	Impact energy (ft-lb)	Remarks	Impactor X location (in.)	Impactor Y location (in.)
0	NA	B 001	< 1	Background	NA	NA
1	1	B 002	6	Left Side	-42.625	30.5
2	1	B 003	6		-43.125	30.5
3	1	B 004	6	fiber breakage observed	-42.25	30.5
4	1	B 005	6	crack above the impact spot	-42.25	30.5
5	1	B 006	3		-40.94	30.5
6	1	B 007	3		-40.94	30.5
7	1	B 008	3		-40.25	30.5
8	1	B 009	1		-39.75	30.5
9	1	B 010	1		-40	30.5
10	1	B 011	1		-40	30.5
11	2	B 012	1		-34	30.5
12	2	B 013	1		-34	30.5
13	2	B 014	1		-35	30.5
14	2	B 015	3		-34.375	30.5

Test No.	Location Map	Strain Gage and File No	Impact energy (ft-lb)	Remarks	Impactor X location (in.)	Impactor Y location (in.)
15	2	B 016	3		-33.625	30.5
16	2	B 017	3		-33.75	30.5
17	2	B 018	6		-33.5	30.5
18	2	B 019	6	fiber breakage observed	-33.5	30.5
19	2	B 020	6		-31.5	30.5
20	3	B 021	6	Right Side	122.75	-30.5
21	3	B 022	6		122.25	-30.5
22	3	B 023	6		121.125	-30.5
23	3	B 024	3		120.1875	-30.5
24	4	NA	3		73.375	-30.5
25	4	NA	3		73.5	-30.5
26	4	NA	3		72.75	-30.5
27	4	NA	6		73.5	-30.5
28	4	NA	6		72.25	-30.5
29	4	NA	6		71.5	-30.5
30	5	A 025	6	Cork	81.375	-30.5
31	5	A 026	6	Cork	81.375	-30.5
32	5	A 027	6	Cork	80.375	-30.5
33	6	A 028	6		21.375	-30.5
34	6	A 029	6		21	-30.5
35	6	A 030	6		20.25	-30.5
36	6	A 031	3		19.25	-30.5
37	6	A 032	3		19	-30.5
38	6	A 033	3		18.5	-30.5
39	7	A 034	3		-71.125	-30.5
40	7	A 035	3		-70.25	-30.5
41	7	A 036	3		-69.625	-30.5
42	7	A 037	6		-74.188	-30.5
43	7	A 038	6		-74.75	-30.5
44	7	A 039	6		-74.188	-30.5
45	8	A 040	3	Left Side	-40	30.5
46	8	A 041	3		-41	30.5
47	8	A 042	3		-41.375	30.5
48	8	NA	3		-39.125	30.5
49	9	A 043	3		16.25	30.5
50	9	A 044	3		16.5	30.5
51	9	A 045	3		17	30.5
52	9	A 046	1		17.75	30.5
53	9	A 047	1		17.625	30.5
54	9	A 048	1		16.875	30.5
55	9	A 049	3		14.5	30.5
56	9	A 050	3		15.5	30.5

Test No.	Location Map	Strain Gage and File No	Impact energy (ft-lb)	Remarks	Impactor X location (in.)	Impactor Y location (in.)
57	9	A 051	3		14.125	30.5
58	9	A 052	3		15	30.5
59	9	A 053	6		14.125	30.5
60	9	A 054	6		14	30.5
61	9	A 055	6		15.25	30.5
62	10	A 056	3		51.25	30.5
63	10	A 057	3		51.125	30.5
64	10	A 058	3		51.375	30.5
65	10	A 059	6		52.25	30.5
66	10	A 060	6		52	30.5
67	10	A 061	6		52.375	30.5
68	11	A 062	3		61.625	30.5
69	11	A 063	3		60.875	30.5
70	11	A 064	3		61.375	30.5
71	11	NA	3		61.875	30.5
72	11	NA	3		62.5	30.5
73	11	A 065	6		62	30.5
74	11	A 066	6		63.25	30.5
75	11	A 067	6		63.5	30.5
76	12	A 068	6	Extreme Tail	-176.5	30.5
77	12	A 069	6		-176.5	30.5
78	12	A 070	6		-175.5	30.5
79	12	NA	6		-175	30.5
80	12	NA	6		-174.75	30.5
81	12	NA	6		-174.75	30.5

The experimental map (Figure 1) splits the motor into sides; top, bottom, left and right (bottom side not plotted). With the motor on the chocks, the nozzle is angled towards the ground and this defines the bottom. Since the impactor hits the midline of the case, all impact points are in the center of either the left or right side. All dimensions and distances are inches measured along the surface. The three gages within one rosette are defined in terms of their orientation. The "X" gage is along the axial direction, the "L" gage is parallel to the circumferential direction and the "XL" gage is oriented at 45 degrees to both the axial and circumferential axes. I have included in the table the impact positions for which strain gage waveform data was recorded, the data file name and the gage used. Although not presented, the data are available for further analysis and in many cases, comparable impact strain data were also recorded on the empty case.

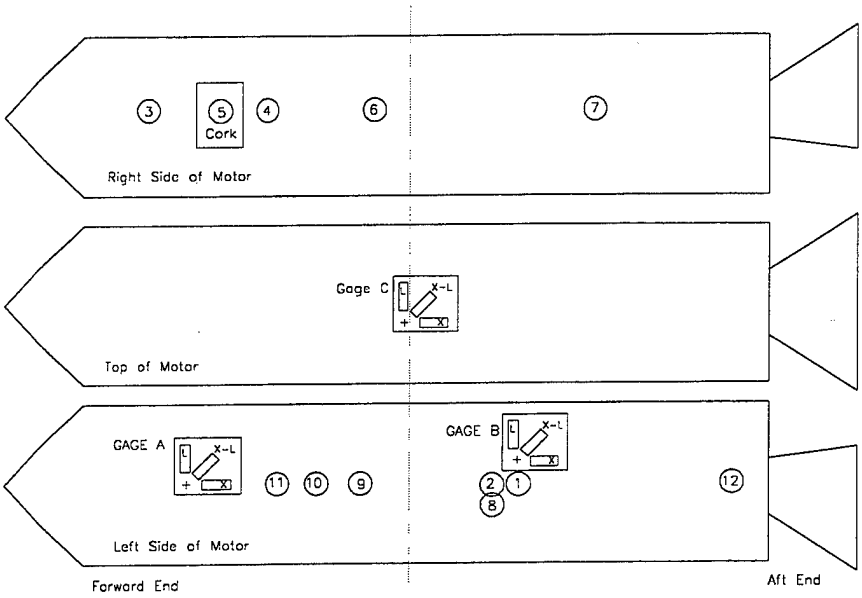

Figure 1. Relative locations of GEM motor strain gages and impacts.

3. Data and Results

Figure 2 shows three representative strain waveforms from one location and three different energies. These data are from impact location 1, and the data are from gage B-L. This gage is located along a circumferential line, 17 in. from the impact. Although data were recorded from all three gages on the rosette, only the gage aligned with the impact spot to gage centerline is presented in this plot. The three impact energies are nominally 1, 3, and 6 ft-lb. The impact force was measured simultaneously and recorded with the strain data. The data show essentially a single sharp impulse followed up by much lower amplitude, low-frequency ringing. The structure of both the strain impulse and the low-frequency ringing is extremely reproducible. Multiple impacts were done at each energy, and the shot-to-shot wave shapes are virtually identical. The wave shape does not change with increasing impact energy, and the peak height scales roughly linearly with impact energy. Impact energies above 7 ft-lb are expected to cause damage to the case. For this reason, 6 ft-lb was the maximum impact energy used. I would expect the wave shape to change with impact energies above the case damage threshold and to see a sublinear increase in amplitude. The wave shapes from the three different gages on the rosette (not presented) are all visually distinctive from each other, and reproducible. Interpretation of the waveforms is beyond the scope of this report.

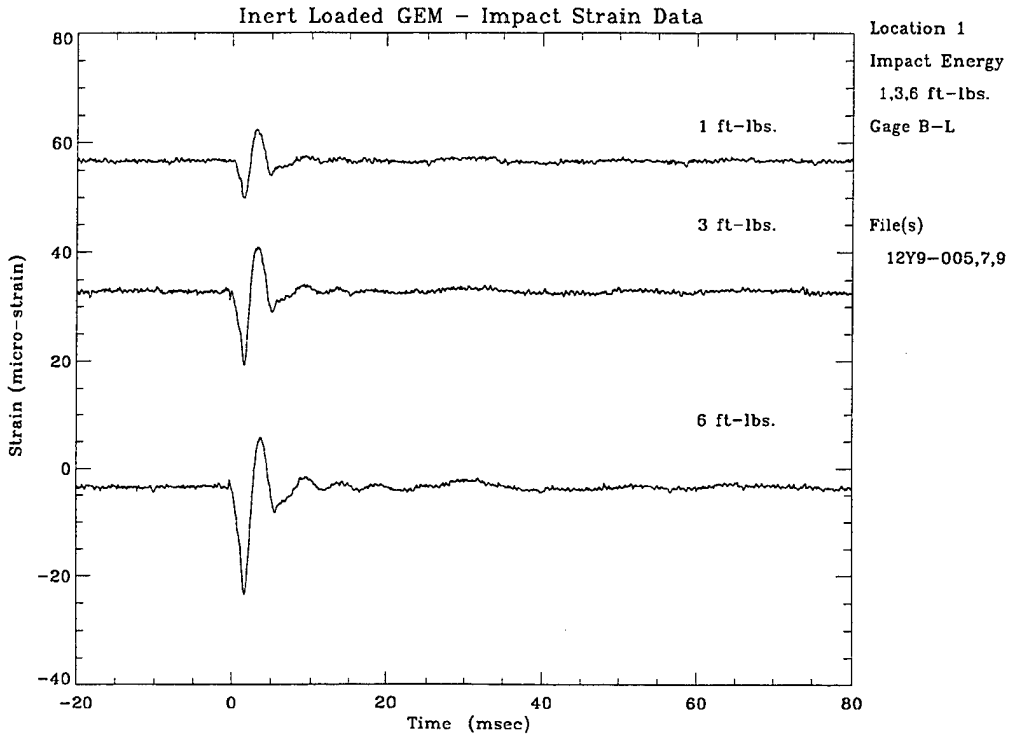

Figure 2. Strain impulse for three different impact energies.

Figure 3 re-plots the 3 ft-lb impact waveform from Figure 2 at an extended time scale, along with a representative strain wave from an impact on the empty case. This empty case impact was nominally 3 ft-lb, and the impact-gage geometry is fairly close to the inert loaded case, gage B-L, impact location 1. All of the empty-case waveforms are much larger in amplitude than the loaded-case waveforms and extremely complex. For the empty case, the waveform fine structure is very reproducible, and the signals from each gage on the rosette have distinctive fingerprints. These strain waves appear to be damped ringing waveforms with frequency components nominally within the 50 to 200 Hz range. This shows that one cannot predict the Gr/Ep surface impact strain signatures based on empty-case impact data without a rigorous understanding of the overall mechanical structure.

An attempt was made to measure the damping of the waveform as the impact is axially removed from the strain gage. Figure 4 shows impacts at 6 ft-lb for four different axial distances from the gage. The data presented are only from gage A-X. This gage was oriented parallel to the motor axial dimension and located near the center of the motor's left side. This provides for a linear-axial wave propagation path (from several impacts to the gage) without a circumferential component. The top trace impact is 6 in. from the gage. The next trace down is at 17 in. from the gage, and the impulse spike is about 1/4 of the amplitude of the top trace. The third trace is 52 in. from the gage, and the impulse spike is virtually gone. The lower-frequency ringing component is not damped nearly as much as the sharp impulse spike. This is more obvious when the data are plotted out to the full 800 ms. The bottom trace is from an impact near the tail of the motor, 243 in. from the gage. The amplitude of this trace is about half that from an impact 20% of this distance from the gage. Only the top two plots have sufficiently well defined impulse spikes for wave propagation time measurements. The relative peak separation is too small in relation to the peak widths and the width of the impact impulse to make an accurate measurement of the wave velocity.

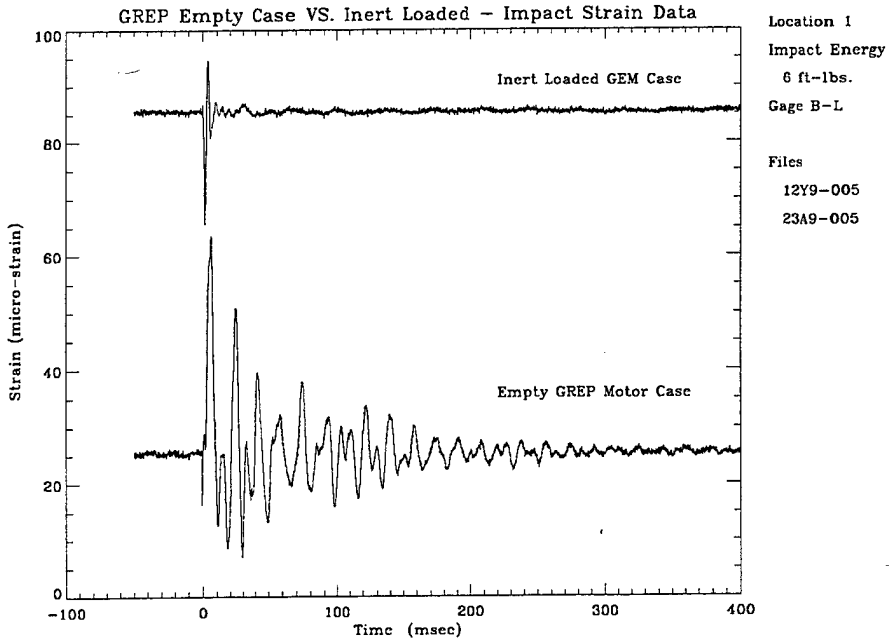

Figure 3. Comparison of strain waves propagated in an empty case and the inert-propellant-loaded GEM.

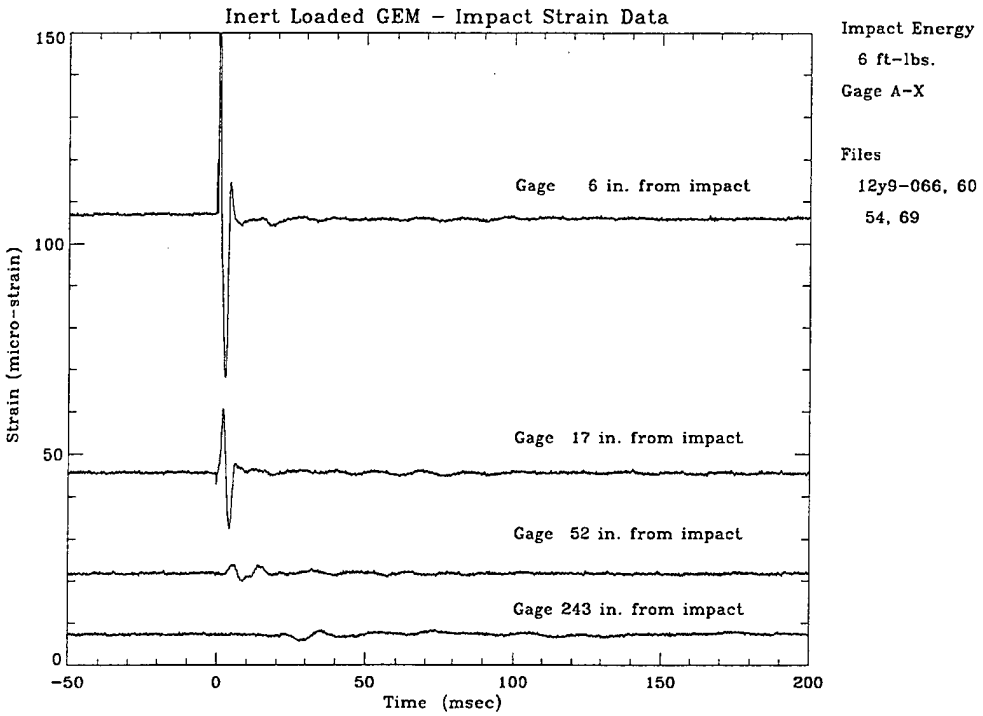

Figure 4. Axial strain-wave propagation at different gage-to-impact distances.

Figure 5 is a semi-random collection of waveforms from impacts geometrically removed from the sensing gage (i.e., impacts on the other side of the motor case). This plot is extended out to 400 ms since there are no impulse spikes observed, and the longer time plot better shows the low-amplitude ringing. The top trace is from a 6-ft-lb impact at location 3, gage B-L. With the exception of the tail hit, this was the farthest removed (210 linear inches) impact to strain gage combination tested. This impact-to-gage distance is roughly comparable to the maximum possible gage-impact distance, assuming one were to mount a single gage at the motor midline. A 3-ft-lb impact was also recorded for this impact-gage location, and the signal was still above the noise floor. The middle trace is from a 6-ft-lb impact at location 5 (hitting on the cork), a distance of 77 in. from the gage and recorded with gage A-LX. The next trace (2nd from bottom) is from a 6-ft-lb impact location 7, gage A-LX. This impact is a net linear distance of 204 in. from the impact to the gage. The bottom trace is another "tail hit" waveform, monitored with gage A-L and an impact distance of 243 in.

Lifting, handling, and transportation strain signals were also monitored. Any attempt to extract impact data from dynamic strain measurements needs to be able to separate impact signals from background transportation and handling strains. A third strain gage (gage C) was located at the top center of the motor case for measuring the maximum strains with various lifting stresses. A maximum axial strain difference of 500 micro-strain was measured from the motor at rest in the chocks to a single-point lift at the center of the motor. This strain is huge relative to the ±10 micro-strain signals from the impacts. Furthermore, dynamic strain oscillations of ±25 micro-strain were recorded when the motor was set back into the chocks from a lift position. A background strain of 80 micro-strain was recorded when the motor case was tied down to a flatbed truck with ratchet straps. The ratchet straps typically "pop" when released. This would probably cause a large strain impulse to be

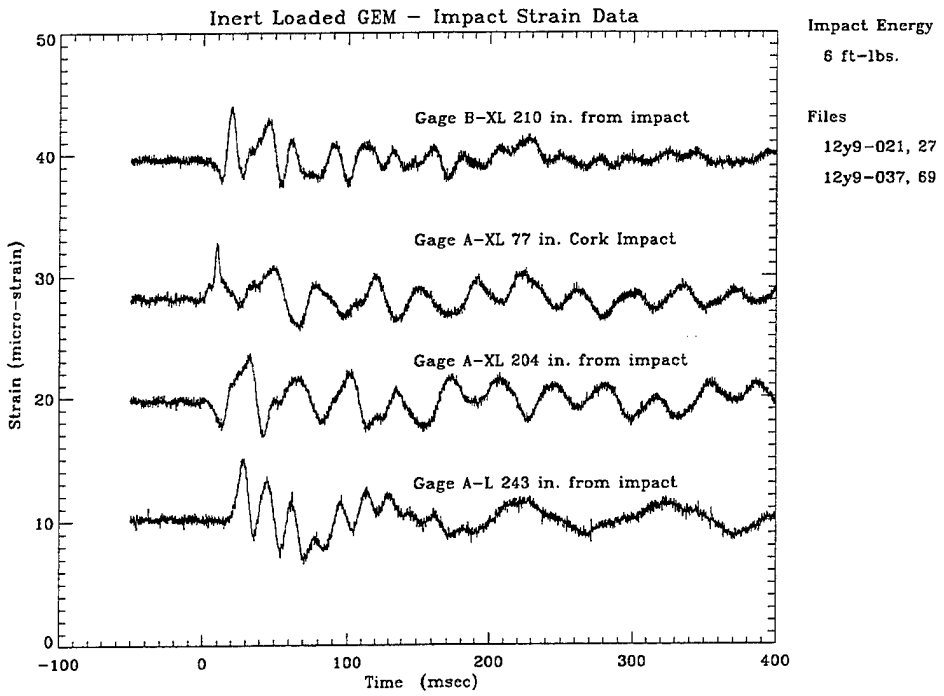

Figure 5. Assortment of strain waves from different impact-gage geometrical combinations.

launched into the motor. An attempt to record this impulse was made. However, the trigger timing was not successfully coordinated, and no results are available.

Road strains were recorded by driving the loaded flat-bed over a set of wooden 2 x 4's at approximately 15 mph. Figure 6 shows a very dynamic, oscillating strain signal induced by the 2 x 4 bumps. The peak amplitudes are ±150 micro-strain with a frequency of about 10 Hz. Also shown in the figure is a trace with the truck stopped, but still running. The high background noise is believed to be RF coupled into the first-stage pre-amplifier from a nearby DC-to-AC converter. This RF noise problem was much worse before including a 100 Hz low-pass filter on the signal line.

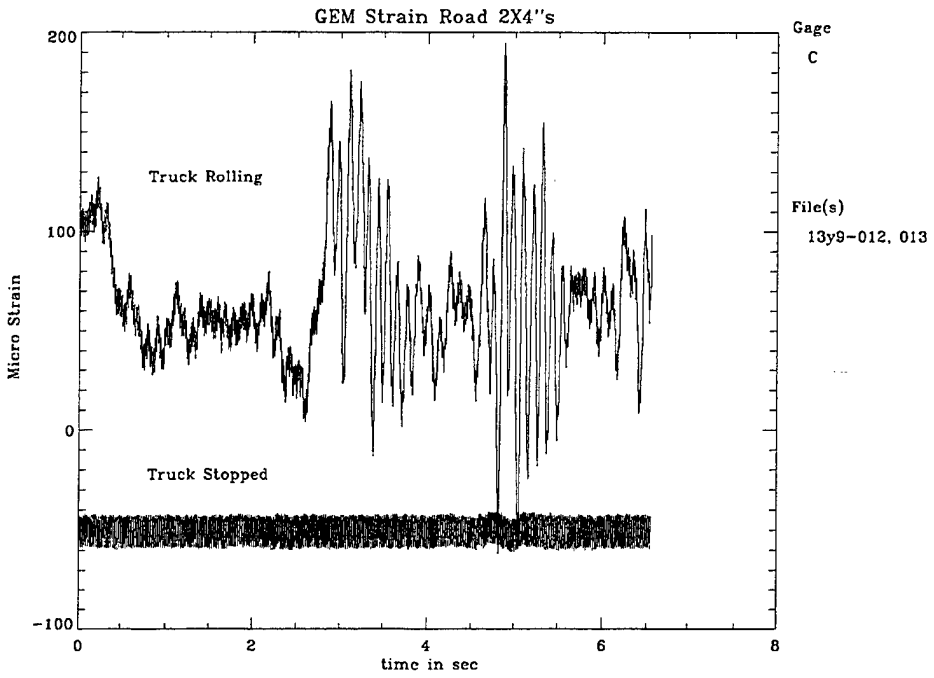

Figure 6. Log of GEM strain during transportation and running over a wood 2 x 4.

4. Discussion

At impact energies below damage threshold, very reproducible strain waves and impulses are launched into the Gr/Ep motor cases. These strain waves are relatively large in magnitude and can be easily sensed by conventional resistance strain gages located fairly far from the impact location. The sharp impulse signal magnitudes track reliably with impact energy, and the low-frequency ring-down signals that follow the impulses are distinctive and reproducible. However, predicting these signatures, especially in view of the dramatic difference between the empty case and the inert loaded case, would require a very sophisticated understanding of the Gr/Ep case-propellant structure. Other parameters such as impactor geometry, impact angle, etc. are also expected to change the waveform signatures.

The background strains from lifting, handling, and transportation were large relative to the impact strain signals. This could make impact identification and waveform interpretation difficult under non-static conditions. Presumably, the road-bump, flat-bed truck transportation environment used in this test series is much more severe than the flight GEMs are subjected to. The data do serve to illustrate the inherent difficulty of separating a small fast transient from large non-static signals.

There is the potential to extract more information from this dataset. Power spectral density analysis of the impact waves or motor flexing with road bumps may be of value. This is, however, beyond the scope of this report. A large set of "empty case" impact data also exists. The digital data, along with a digitized signal from a load cell on the deadweight impactor, are available on request.

TECHNOLOGY OPERATIONS

The Aerospace Corporation functions as an "architect-engineer" for national security programs, specializing in advanced military space systems. The Corporation's Technology Operations supports the effective and timely development and operation of national security systems through scientific research and the application of advanced technology. Vital to the success of the Corporation is the technical staff's wide-ranging expertise and its ability to stay abreast of new technological developments and program support issues associated with rapidly evolving space systems. Contributing capabilities are provided by these individual organizations:

Electronics Technology Center: Microelectronics, VLSI reliability, failure analysis, solid-state device physics, compound semiconductors, radiation effects, infrared and CCD detector devices, data storage and display technologies; lasers and electro-optics, solid state laser design, micro-optics, optical communications, and fiber optic sensors; atomic frequency standards, applied laser spectroscopy, laser chemistry, atmospheric propagation and beam control, LIDAR/LADAR remote sensing; solar cell and array testing and evaluation, battery electrochemistry, battery testing and evaluation.

Mechanics and Materials Technology Center: Evaluation and characterizations of new materials and processing techniques: metals, alloys, ceramics, polymers, thin films, and composites; development of advanced deposition processes; nondestructive evaluation, component failure analysis and reliability; structural mechanics, fracture mechanics, and stress corrosion; analysis and evaluation of materials at cryogenic and elevated temperatures; launch vehicle fluid mechanics, heat transfer and flight dynamics; aerothermodynamics; chemical and electric propulsion; environmental chemistry; combustion processes; space environment effects on materials, hardening and vulnerability assessment; contamination, thermal and structural control; lubrication and surface phenomena.

Space and Environment Technology Center: Magnetospheric, auroral and cosmic ray physics, wave-particle interactions, magnetospheric plasma waves; atmospheric and ionospheric physics, density and composition of the upper atmosphere, remote sensing using atmospheric radiation; solar physics, infrared astronomy, infrared signature analysis; infrared surveillance, imaging, remote sensing, and hyperspectral imaging; effects of solar activity, magnetic storms and nuclear explosions on the Earth's atmosphere, ionosphere and magnetosphere; effects of electromagnetic and particulate radiations on space systems; space instrumentation, design fabrication and test; environmental chemistry, trace detection; atmospheric chemical reactions, atmospheric optics, light scattering, state-specific chemical reactions and radiative signatures of missile plumes.

Center for Microtechnology: Microelectromechanical systems (MEMS) for space applications; assessment of microtechnology space applications; laser micromachining; laser-surface physical and chemical interactions; micropropulsion; micro- and nanosatellite mission analysis; intelligent microinstruments for monitoring space and launch system environments.

Office of Spectral Applications: Multispectral and hyperspectral sensor development; data analysis and algorithm development; applications of multispectral and hyperspectral imagery to defense, civil space, commercial, and environmental missions.